Molecular arrangements and reorientation behavior in a dibenzopyrene-derivative ferroelectric columnar liquid crystal as studied by time-resolved Fourier-transform ir spectroscopy

S. V. Shilov
Institute of Macromolecular Compounds, Bolshoi prospekt 31, 199004 St. Petersburg, Russia
and Department of Physics and Geosciences, University of Leipzig, Linnéstrasse 5, 04103 Leipzig, Germany

M. Müller, D. Krüerke, and G. Heppke
Iwan-N.-Stranski-Institute, Technical University of Berlin, Sekretariat ER11, Strasse des 17 Juni 135, 10623 Berlin, Germany

H. Skupin and F. Kremer
Department of Physics and Geosciences, University of Leipzig, Linnéstrasse 5, 04103 Leipzig, Germany
(Received 6 May 2001; revised manuscript received 21 September 2001; published 25 January 2002)

Polarized, time-resolved Fourier-transform infrared spectroscopy was employed to study the orientational order and the reorientation dynamics of a diskotic ferroelectric liquid crystal. In the shear oriented cell the dibenzopyrene derivative forms two different field-dependent columnar phases that show a tripling in the spontaneous polarization. These field-dependent phases are analyzed with respect to the dependence of the infrared absorbance from the polarization plane. In this way it was confirmed that the high-field phase is characterized by a homogeneous orientation of the tilt-plane formed by the core normals $\vec{n}$ and the column axis $\vec{N}$. In contrast, in the low-field phase the columns exhibit several different tilt-planes. The orientational order parameter of the columns is determined. It was also detected that the average orientation of the alkyl tails of the molecules is not lying in the plane of the disklike core. By monitoring the evolution of the infrared bands in the course of the electric-field-induced reorientation, we found that the reorientation process is divided into three steps: A fast initial response followed by a slowing down of the reorientation is observed, which then is followed by an acceleration of the reorientation. In the high-field phase the fast initial electrical induced process can be assigned to a rotation of the molecules around the column axis by a few degrees. During the subsequent ferroelectriclike response the molecules rotate around the column axis by approximately 180°. Other models for this switching mechanisms could be excluded.

DOI: 10.1103/PhysRevE.65.021707 PACS number(s): 61.30.Gd, 78.47.+p, 78.30.−j

I. INTRODUCTION

In 1981 Prost proposed that the main prerequisites for the appearance of ferroelectricity in columnar mesophases are the chirality of the molecules and the occurrence of a tilt of the individual molecules with respect to the column axis $\vec{N}$ [1] (Fig. 1). This suggestion was first realized experimentally by Bock and Helfrich who described bistable ferroelectric switching for some dibenzopyrene derivatives in 1992 [2]. Subsequently, columnar ferroelectrics were synthesized by Scherowsky and Chen [3] and Heppke *et al.* [4]. It was found that some dibenzopyrene derivatives [2,5] and their mixtures [5] exhibit different phases in dependence of the external electric-field strength. The ''low-field phase'' (for electric fields less than 10 V/μm) shows a smaller spontaneous polarization and smaller reorientation angles of the optical axis than the ''high-field phase.'' Based on the assumption of a quasihexagonal lattice Ref. [6] describes tentative structures of these phases with four columns in each unit cell. A detailed study with x ray and synchrotron radiation shows that the structure of the low-field phase is characterized by a rectangular unit cell containing six columns [7]. Although detailed information about the crystallographic structure is present, an analysis of the segmental arrangements has not been given yet.

Three possible mechanisms of switching in columnar ferroelectrics were suggested in Refs. [2,3,6]. In one case, the molecules rotate around the axis $\vec{N}$ of the column. In another case the tilt of the disk normals $\vec{n}$ with respect to the column axis $\vec{N}$ reverses through an untilted state with no molecular rotation around the column axis. According to a third mechanism the molecular tilt direction, but not the molecules themselves, rotate around the column axis. To date, it is unknown

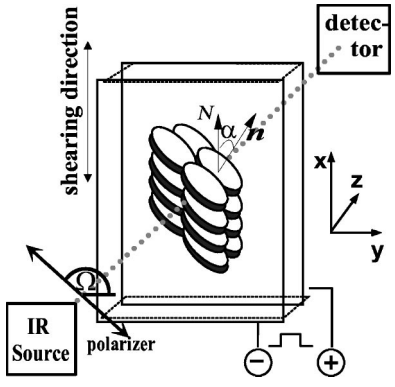

FIG. 1. Scheme of the experimental setup. The polarizer angle Ω, the normal of the core disk $\vec{n}$, the column axis $\vec{N}$, the tilt angle α, and the laboratory coordinate system x,y,z are indicated. The direction of the polarization vector at $\Omega=90°$ corresponds to the shearing direction.

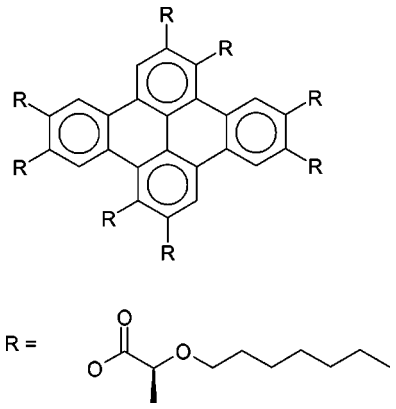

FIG. 2. Chemical structure of the dibenzopyrene under study. The phase sequence is Cr $\overset{70\,^\circ}{\rightarrow}$ Col $\overset{126\,^\circ}{\leftrightarrow}$ Iso. Upon cooling, no crystallization is observed.

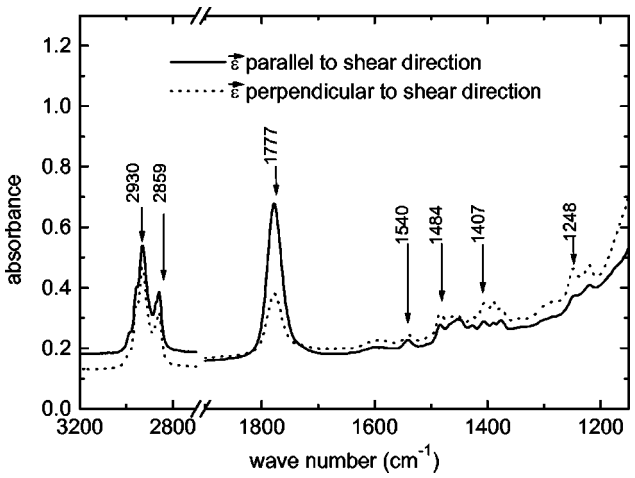

FIG. 3. ir spectra of a freshly sheared sample at $E=0$ V/μm for two different ir polarization planes.

which mechanism dominates in ferroelectric switching.

A powerful tool for studying the segmental orientations in organic materials is the Fourier-transform infrared (FT-ir) spectroscopy. Recently FT-ir spectroscopy with unpolarized light was used to analyze the electric-field-induced phase transition in a ferroelectric dibenzopyrene [8]. The dependence of the intensity of the C=O band on the electric field as observed in this reference cannot be explained by the model for the high-field phase suggested in Ref. [6]. More specific information about the orientation of the different moieties under application of a static external electric field can be extracted, if the ir absorbance is measured with polarized light of different polarization planes [9]. Its combination with time-resolved FT-ir spectroscopy allows us to follow the molecular motion in the course of the ferroelectric switching [10–13].

In order to establish the segmental arrangements in the low- and the high-field phase and to elucidate the mechanism of the molecular reorientation, we studied by FT-ir spectroscopy the orientation of the molecular moieties in columnar ferroelectric liquid crystals under the influence of external static and alternating electric fields.

II. EXPERIMENT

The experimental setup for the ir experiments and the chemical structure of the investigated substance 1,2,5,6,8,9,12,13-octakis[(*S*)−2 heptyloxy]dibenzo[*e*,*l*]pyrene (D8m*10) are shown in Figs. 1 and 2, respectively. The columnar phase is found within the temperature interval from 70 to 126 °C. The sample was oriented by shearing the liquid crystalline melt (at 110 °C) between CaF_2 windows coated with an ITO (indium tin oxide) layer in order to make the surface conductive. An additional SiO layer protects the ITO electrodes from short circuits. Polyethylenterephtalate spacers with a thickness of 2 μm were used to maintain a well defined spacing between the electrodes.

The FT-ir spectrometer (FTS-6000, Bio-Rad) was accomplished with an ir microscope (UMA-500, Bio-Rad). The sample was positioned on the microscope stage in the visible light mode of the microscope using crossed polarizers. A sample region of uniform orientation (200 μm×200 μm) was selected for the ir measurements. After sample positioning, the microscope was switched from the visible light mode to the ir mode. The propagation direction (laboratory *z* axis) of the polarized ir beam was perpendicular to the plane of the windows (*x*-*y* plane, Fig. 1). ir spectra were measured as a function of the polarizer rotation angle Ω from 0 ° to 170 ° in steps of 10 °. For each band under study the polarization dependent absorbance is fitted according to Eq. (A14) (Appendix). This allows to determine the positions (Ω_0 and $\Omega_0+90\,^\circ$) of maximal and minimal absorbance with a precision of approximately $\pm 1\,^\circ$. The polarization vector at Ω_0 determines the ''apparent'' average orientation of the corresponding transition moments, where ''apparent'' means that just the vector components perpendicular to the ir-propagation count. Therefore, a shift in the $A(\Omega)$ curves that appear in response to the alternating external electric field reflects a reorientation of the corresponding molecular segments. The dichroic ratio *R* of the selected bands was calculated as the ratio of the maximum and minimum in the polarization dependent absorbance curve: $R=A(\Omega_0)/A(\Omega_0+90\,^\circ)=A_{max}/A_{min}$.

For measurements under the influence of a static external electric field, the ir spectra of the sample were recorded in the routine rapid-scan mode of the FTS-6000 with a spectral resolution of 4 cm^{-1}. In order to collect time-resolved spectra in course of the molecular reorientations in response to an alternating external electric field the step-scan technique was used. The scheme of the driving signals in the step-scan mode is described elsewhere [14]. Time-resolved spectra have been recorded with a time resolution of 5 μs and a spectral resolution of 8 cm^{-1}.

The measurements in the visible range were made in a setup principally similar to the ir setup: The transmission of the sheared sample was monitored by means of a photomultiplier on top of a polarizing microscope. Its signal output was recorded by a digital oscilloscope.

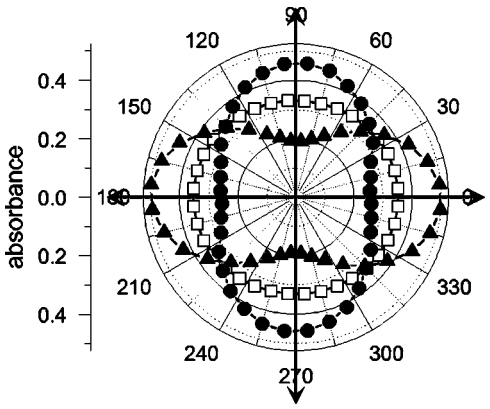

FIG. 4. Polar plot of the ir absorbance vs ir polarizer angle A_Ω for the 2930 cm^{-1} band (CH_2, open square symbol), the 1777 cm^{-1} band (CO, circle symbol), and the 1407 cm^{-1} band (core, triangular symbol). The dibenzopyrene sample is freshly sheared and no external electric field is applied. The absorbance at 1407 cm^{-1} is multiplied by 6. The direction of the polarization vector at $\Omega = 90°$ corresponds to the shearing direction.

III. RESULTS AND DISCUSSION

A. Molecular orientation without field

The ir spectra of a freshly sheared sample at 110 °C are shown in Fig. 3 for two different polarization vectors. The ir absorbance versus polarizer angle A_Ω for selected bands is plotted in Fig. 4. The tentative assignments of some ir-absorption bands are given in Table I (second column). To derive information about segmental orientation from ir spectra in polarized light one needs to know the direction of the ir transition moment for the corresponding band relative to the molecular axes. It is well known that the transition moment for the carbonyl band at 1777 cm^{-1} is directed nearly along the C=O bond. The bands assigned to the CH_2 groups in the alkyl tails at 2930 and 2859 cm^{-1} have the transition moment perpendicular to the alkyl chain in all-trans conformation. The transition moments of bands at 1540, 1484, and 1407 cm^{-1} (molecular core) are nearly in the plane of the core.

As can be seen from Figs. 3 and 4 the bands assigned to the core show perpendicular dichroism ($A_{0°} = A_{max} > A_{90°} = A_{min}$), where $A_{0°}$ and $A_{90°}$ are the peak absorbances at $\Omega = 0°$ and $\Omega = 90°$, respectively) while bands due to alkyl chain and carbonyl show parallel dichroism ($A_{0°} = A_{min} < A_{90°} = A_{max}$). Taking into account the directions of transition moments for these bands it is possible to conclude from the dichroism that the core plane and the axes of the alkyl tails orient in average perpendicular to the shearing direction. The same result was obtained from optical measurements [15]. From that one can conclude that the axis of the columns $\vec{N}$ formed by the molecular cores points parallel to the shear direction. The dichroic ratios are given in Table I. The value $R = 1.09$ (close to value $R = 1$ that is characteristic for isotropic orientation) for CH_2 bands proves a weak orientation of the CH_2 groups.

TABLE I. Band assignment, dichroic ratios R, and apparent tilt angles Θ for the different-field dependent phases of the dibenzopyrene derivative D8m*10.

Band position (cm^{-1})	Assignment	No field	Low-field phase		High-field phase	
		R	R	$\Theta/°$	R	$\Theta/°$
2930	ν_{as} (CH_2)	1.06	1.09	4.0	1.09	9.1
2859	ν_s (CH_2)	1.10	1.12	2.5	1.12	5.0
1777	ν (C=O)	2.60	3.25	13.3	6.32	25.2
1540	ν $(C—C)_{ar}$	1.06	1.59	45.0	4.47	43.0
1484	ν $(C—C)_{ar}$	1.28	1.75	31.8	3.05	38.3
1407	ν $(C—C)_{ar}$	1.80	1.64	18.3	3.18	30.2
1248	ν_{as} (C—O—C)	2.69	3.03	13.1	6.23	24.3

B. Molecular orientations in the low-field phase

The low-field phase for D8m*10 is formed at a field strength $E \leqslant 10$ V/μm. Bistable ferroelectric switching was observed in this phase, if the polarity of the external field is reverted. The different molecular orientations for a positive and negative electric field are demonstrated by the polar plots of the ir absorbance vs polarizer angle $A(\Omega)$ [Fig. 5(a,b)]. For the different bands the polarizer angles for which extremum absorbance is obtained (either Ω_0 or $\Omega_0 + 90°$) are no longer zero. Furthermore Ω_0 (or $\Omega_0 + 90°$) for positive and for negative voltage differ in their signs but have the same absolute value. This absolute value is called the "apparent angle Θ" as it denotes the angle of the apparent orientation of the corresponding segment with respect to the column axis $\vec{N}$, which is represented by $\Omega = 90°$. The "apparent angle" is maximal for the 1484 cm^{-1} core band ($\Theta \approx 32°$) while it is minimal for the 2930 cm^{-1} band (CH_2 tails). The nonzero values for Θ_{2924} and for Θ_{1484} prove that neither the average alkyl tail nor the core plane are oriented any longer perpendicular to the shearing direction and hence to the column axis $\vec{N}$. The difference in these two Θ values shows that the alkyl chains and the plane of the core are inclined to each other as well [11]. This result supports the conjecture concerning tail deflection made in Ref. [2].

The apparent Θ angles and dichroic ratios for selected bands obtained from absorption versus polarization plots are summarized in Table I (columns 3 and 4). Analyzing this table one can observe that the Θ values for the bands assigned to the core (1540, 1484, 1407, and 1248 cm^{-1}) are different from each other. As shown earlier [15] the difference in apparent angles results from the noncylindrical symmetry of the orientation distribution function of ir transition moments around the normal of the core plane $\vec{n}$. The core bands exhibit low values of the dichroism of the core bands (Table I). This may ascribe to different directions of the cores in neighboring columns [Fig. 5(c)] as proposed earlier [6,7]. The corresponding models for the different column orientations are discussed in conjunction with the field-induced phase change in the next section.

C. Molecular orientations in the high-field phase

The transition to the high-field phase is observed in an external electric field $E > 10$ V/μm. Polar plots of the ir

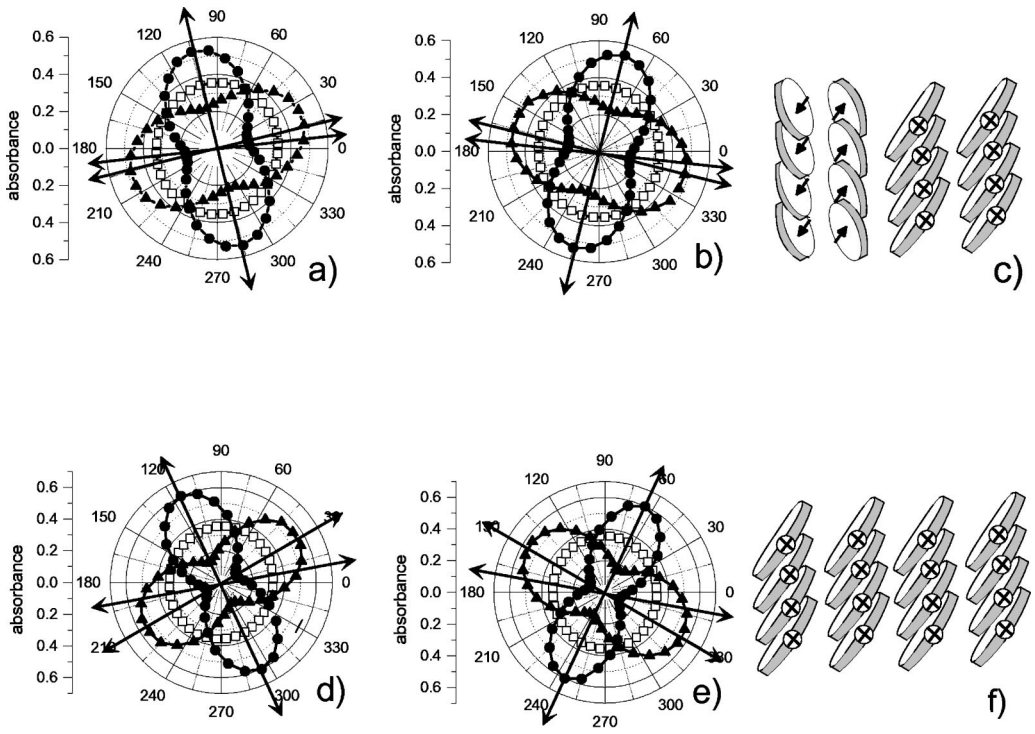

FIG. 5. Polar plots of the ir absorbance vs ir polarizer angle A_Ω for the 2930 cm^{-1} band (CH_2, open square symbol), the 1777 cm^{-1} band (CO, circle symbol), and the 1407 cm^{-1} band (core, triangular symbol). The results are shown for dibenzopyrene in the low-field phase at $E=+9$ V/μm (a) and at $E=-9$ V/μm (b) and in the high-field phase at $E=+20$ V/μm (d) and at $E=-20$ V/μm (e). The columns in the low-field phase have differently oriented tilt planes (c), whereas in the high-field phase (f) a homogeneous orientation of the columns can be deduced. The viewing direction of the sketches (c) and (f) is normal to the cell windows.

absorbance vs polarizer angle are shown in Figs. 5(d) and 5(e) for positive and negative external electric fields. The apparent tilt angles Θ and dichroic ratios R for selected bands are given in Table I. The transition to the high-field phase results in an increase of the Θ values for all molecular segments. This is in accordance with the earlier described electro-optical observation of higher tilt angles in the high-field phase [2,6]. Similar to the low-field phase the differences in the Θ values for bands assigned to the alkyl (2930 and the 2859 cm^{-1}) and those assigned to the core reflect the deflection of alkyl chains with respect to the core plane. The noncoincidence of the Θ values for the different core bands is again due to the biased rotation of the core around its axis $\vec{n}$.

In addition to the apparent angles, the dichroic ratios R for the different bands are also considerably higher for the high-field phase than for the low-field phase. A detailed analysis of x-ray and synchrotron scattering data led to sixteen possible crystallographic structures for the low-field phase [7]. Their unit cells contain six discotic columns that are pointing to four or five different directions, respectively [Fig. 6(b)]. The columns can be characterized by the angle ϕ of their polarization vector with respect to the macroscopic spontaneous polarization of the entire phase [Fig. 6(a)]. Due to the different orientation of the columns, their molecular dipoles are partly averaged out and the macroscopic spontaneous polarization in all of the proposed structures are one third of the structure with homogeneous column orientation [Fig. 6(c)]. From the fact that the spontaneous polarization of the high-field phase was measured to be three times larger than those of the low-field phase, it was deduced that the high-field phase is characterized by the homogeneous orientation of the columns [7].

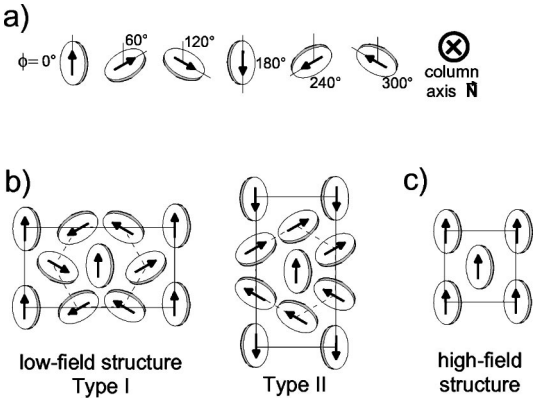

FIG. 6. (a) Sketch of the six types of columns differing in the orientation of their tilt plane. Only one disk per column is drawn, since the viewing direction is along the column axis. (b) Two of the sixteen different structures for the low-field phase derived from Ref. [7]. For the infrared measurements these structures can be classified into two types containing either five (Type I) or four (Type II) differently oriented columns. The absorbance ellipsoids of each of these structures are described by Eq. (A9). (c) Structure for the high-field phase containing columns with a homogeneous tilt-plane orientation.

D. Quantitative comparison of the polarizer dependent absorbance for the low- and the high-field phases

For the purpose of the analysis of infrared dichroism it is sufficient to regard the number of differently oriented columns in the unit cell of a structure, while the positions of the different columns do not play a role. Consequently, the 16 possible low-field structures derived in Ref. [7] can be classified into two types of structures. Type I classifies structures in which the unit cells contain two columns with dipoles pointing along the macroscopic polarization ($\phi=0\,°$), and one of each column with $\phi=60\,°$, $120\,°$, $240\,°$, and $300\,°$. The unit cells of the structures of Type II contain one column with $\phi=0\,°$ and with $\phi=180\,°$ and two columns with $\phi=60\,°$ and with $\phi=300\,°$, respectively.

For the two types of low-field phase structures and for the high-field phase structure we calculated the dependence of the infrared absorbance from the polarization vector $A(\vec{\epsilon})$ (see Appendix). By fitting the experimental $A(\Omega)$ data with Eq. (A14) one obtains the parameters $\langle\mu_x^2\rangle$, $\langle\mu_y^2\rangle$, and $\langle\mu_x\mu_y\rangle$, which are the average of the product of each two ir transition moment components along the laboratory x and y axis. For the high-field phase Eq. (A4) links these parameters to two principle axes of the absorbance ellipsoid $\langle\mu_\xi^2\rangle$, $\langle\mu_\eta^2\rangle$ and to the tilt angle of the principle ξ axis with respect to the columnar axis $\vec{N}$. By assuming rotational symmetry for the distribution of the transition moments ($\langle\mu_\eta^2\rangle=\langle\mu_\zeta^2\rangle$) the orientational order parameter can be estimated according to

$$S=\frac{1-R_{col}}{1+2R_{col}}\,\frac{1}{0.5(3\cos^2\beta-1)}, \tag{1}$$

where $R_{col}=\langle\mu_\xi^2\rangle/\langle\mu_\eta^2\rangle$ would be the dichroic ratio of an infinite thin sample and β is the angle formed by the core axis $\vec{n}$ and the transition moment of the absorption band.

For an application of Eq. (1) we take the 1248 cm^{-1} band, which is the band with the highest dichroic ratio among the bands assigned to the core. From the fits [according to Eq. (A14)] of the data in Figs. 5(d,e) we obtain for this band: $\langle\mu_\xi^2\rangle=0.015\,09\pm0.0025$, $\langle\mu_\eta^2\rangle=0.094\,04\pm0.0030$, and $\alpha=\Omega_0=24.3\,°\pm1.0\,°$. Assuming rotational symmetry ($\langle\mu_\zeta^2\rangle=\langle\mu_\eta^2\rangle$) and an angle β of the transition moment of $90\,°$, the orientational order parameter becomes $S=0.78\pm0.16$. Order parameters of a similar value are also found in rodlike ferroelectric liquid crystals.

For the low-field phase one has to distinguish between the absorbance ellipsoid, which refers to the coordinate system ξ,η,ζ of a column and that one which refers to the principle axes frame (PAF) x', y', z' in the laboratory system. Taking the values $\langle\mu_\xi^2\rangle$, $\langle\mu_\eta^2\rangle$, and α for the 1248 cm^{-1} band obtained from the high-field phase measurements and inserting them in the Eqs. (A9) and (A17) one should obtain for the same band in the low-field phase

$$\langle\mu_{x'}^2\rangle=0.0269\pm0.0037,$$

$$\langle\mu_{y'}^2\rangle=0.0890\pm0.0035, \tag{2}$$

$$\Omega_0=9.3\,°\pm0.6\,°.$$

These values calculated from the high-field phase data on the basis of the proposed model for the field-induced phase transition should coincide with the measurement results for the low-field phase. For that the low field phase data in Fig. 5(a,b) are fitted according to Eq. (A14),

$$\langle\mu_{x'}^2\rangle=0.0252\pm0.0015,$$

$$\langle\mu_{y'}^2\rangle=0.0820\pm0.0017, \tag{3}$$

$$\Omega_0=13.1\,°\pm0.9\,°.$$

The fact that the results in Eq. (3) exhibit just small deviations from those in Eq. (2) supports the proposed model for the field-induced phase transition. Nevertheless, the deviations indicate that some additional changes in the columnar structure takes place during the transition from the low-field phase to the high-field phase. It should be also noted that the biaxiality of the absorbance ellipsoid (see the next but one paragraph) has not been taken into consideration yet.

E. Orientational dynamics in the high-field phase

To follow the molecular motion during ferroelectric switching we recorded time-resolved ir spectra for a complete set of ir beam polarizations from $\Omega=0\,°$ to $170\,°$. By that we obtained plots of the ir absorbance vs polarizer angle at time intervals of 5 μs during the ferroelectric switching. The evolution of the different apparent angles Θ with time as extracted from the data are plotted in Fig. 7(a). One can state that these $\Theta(t)$ profiles for all selected bands behave similarly: immediately after the field reversion (at $t=0$) the Θ values are decreased by a few degrees, which takes a time of approximately 20 μs [region I, see insert in Fig. 7(a)]. During the following time interval of approx. 200 μs the change in the Θ angles is slowed down (region II). In the region III the molecules reorient to a large angular extent and reach the second stabilized state after approximately 250 μs. Similar observations are made in the polarization microscope [Fig. 7(b)]. Below we will analyze the molecular motion in these regions in detail.

1. Region I

The fast molecular motion in this region is additionally analyzed by following the ir absorbance in response to a triangular electric field of 15 V/μm (2405 Hz) with an offset of 20 V/μm (temperature: 110 °C). Under these conditions the sample is kept in one of the states of the high-field phase. Thus the alternating part of the electric field can induce only small reorientations around this equilibrium position. For a fixed ir polarizer position the corresponding time-resolved absorbance profiles are presented in Fig. 8(a). This figure shows the linearity between the changes in the absorbance and the voltage. Electro-optical studies [Fig. 8(b)] support these findings. Hence this fast molecular motion is not ferroelectric. It may result from small changes in either the

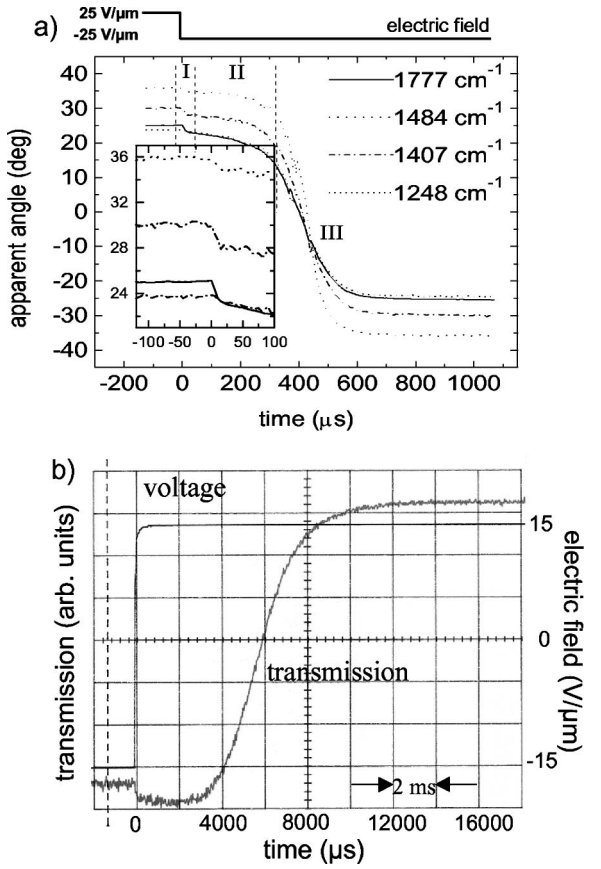

FIG. 7. (a) Time-resolved profiles for the apparent tilt angles for selected absorption bands showing three regions with different molecular mobility. Region I is enlarged in the insert. The polarity of the electric field ($E=\pm 25$ V/μm) is reversed at $t=0$. (b) Optical transmission (white light) of a sheared sample between crossed polarizers in response to a rectangular ac field (approximately ± 15 V/μm, 5 Hz).

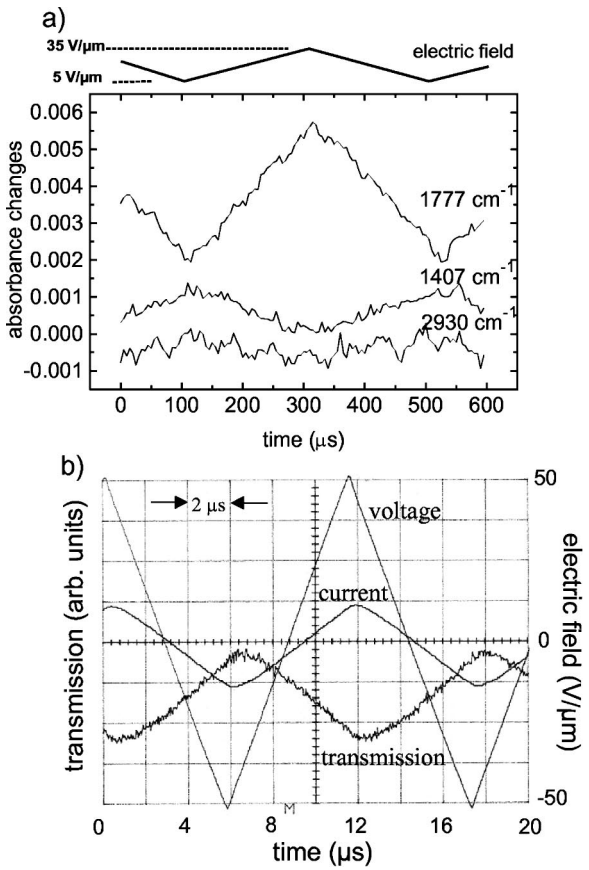

FIG. 8. (a) Absorbance modulation for selected bands due to an electric field showing a linear response on application of a triangular voltage in the high-field phase. The time dependence of the external electric field (ac field ± 15 V/μm, $+20$ V/μm dc bias field) is indicated. (b) Optical transmission (white light) of a sheared sample between crossed polarizers in response to a high-frequency triangular ac field (approximately ± 50 V/μm, 100 kHz; the phase shift is due to the cell capacitance).

azimuthal rotation or the tilt angle of the discotic columns (electrocliniclike). An analysis of the actual reorientation path is given later.

2. Region II

The delay between the field reversal and the reorientation to the second surface-stabilized state for D8m*10 was also observed by electro-optical studies [Ref. [13] and Fig. 7(b)]. It was proposed that this delay in the reorientation in discotic liquid crystals is related to a decomposition of monodomains into smaller domains that are separated by dislocation walls or by melt channels [15].

3. Region III

The switching mechanism in this region is elucidated by a detailed analysis of the time dependence of the absorbance vs polarizer angle plots $A_\Omega(t)$ for the bands assigned to the core. From that the time dependence of the measured dynamic dichroic ratios $R(t)=A_{max}(t)/A_{min}(t)$ and that of the ir absorbances for two fixed polarizations $A_{\Omega=90^\circ}(t)$ and $A_{\Omega=45^\circ}(t)$ are presented in Figs. 9 and 10 correspondingly. Figure 9 shows that R is not constant and reaches a maxi-

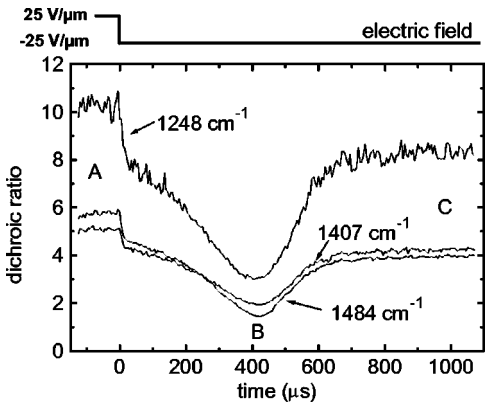

FIG. 9. Time-resolved dichroic ratios for selected bands during the switching from the initial state (A) to the second surface stabilized state (C) via an intermediate state (B).

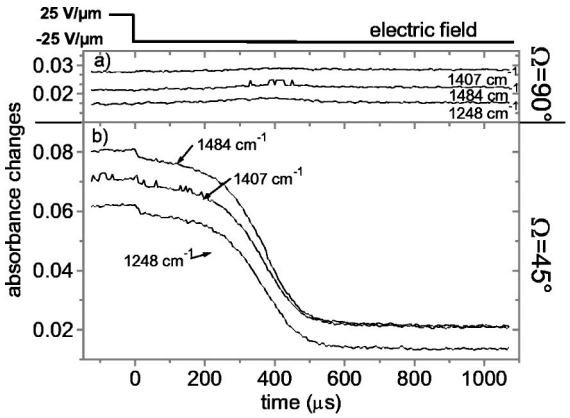

FIG. 10. Time-resolved ir absorbance profiles for the ir polarization vector being parallel to the shearing direction (a) and forming an angle of $\Omega = 45°$ to the shearing direction (b).

mum at $t<0$ (before the field reversal) and at $t>600$ μs (after the reorientation is completed). Approximately 400 μs after the field reversal R reaches its lowest value. While no absorbance change is observed at an ir polarization angle $\Omega = 90°$ [Fig. 10(a)], the maximal change in the absorption is detected at $\Omega = 45°$ [Fig. 10(b)]. It should be noted that for the core bands the absorbance vs polarization plot A_Ω at time $t=0$ (before reversion in polarity) shows higher dichroic ratios (Fig. 9, Table II) than the corresponding A_Ω measurement at a static electric field [Fig. 5(d), Table I]. This indicates an increased orientational order that is obviously caused by the stronger electric field in the time-dependent experiment.

F. Determination of the reorientation path and the biaxiality

An analysis of the absorbance modulation for the different polarizer positions allows one to determine the reorientation path of the discotic columns. For that one has to calculate how the expressions $\langle\mu_x^2\rangle$, $\langle\mu_y^2\rangle$, and $\langle\mu_x\mu_y\rangle$ evolve within the three different models of the reorientation path: (a) through an untilted state, (b) by rotation of the disk normal only, and (c) by rotation of the discotic molecules around the column axis $\vec{N}$ (Fig. 11). For simplicity we neglect the deviations between $\langle\mu_x^2\rangle$ and $A_{\Omega=90°}$, $\langle\mu_y^2\rangle$, and $A_{\Omega=0°}$, $2\langle\mu_x\mu_y\rangle$, and $(A_{\Omega=45=,°}-A_{\Omega=135°})$ that occur due to the final thickness of the sample [Eq. (A13)].

TABLE II. Lengths of the principle axes of different absorbance ellipsoids in the high-field phase of the dibenzopyrene derivative D8m*10 as determined by time-resolved FTIR measurements.

Band position (cm^{-1})	Assignment	$\langle\mu_\xi^2\rangle$	$\langle\mu_\eta^2\rangle$	$\langle\mu_\zeta^2\rangle$
		Error $= \pm 0.001$		
2930	ν_{as} (CH_2)	0.330	0.302	0.304
1777	ν (C=O)	0.533	0.098	0.172
1484	ν $(C—C)_{ar}$	0.015	0.085	0.063
1407	ν $(C—C)_{ar}$	0.015	0.079	0.065
1248	ν_{as} (C—O—C)	0.008	0.079	0.062

The reorientation through an untilted state [Fig. 11(a)] is described by Eq. (A4) when the tilt angle α of the cores is taken as being time dependent: $\alpha=\alpha(t)$. By that, all three expressions $\langle\mu_x^2\rangle$, $\langle\mu_y^2\rangle$, and $\langle\mu_x\mu_y\rangle$ become time dependent, whereas in the PAF description the expressions $\langle\mu_{x'}^2\rangle$, $\langle\mu_{y'}^2\rangle$, and, therefore, the dichroic ratio R remain constant. The experiment shows contrary behavior: $d(A_{\Omega=90°})/dt=0$ and $dR/dt\neq 0$. This allows one to exclude the model of reorientation through an untilted state.

In the second model only the disk normals but not the disks themselves rotate along the column axis [Fig. 11(b)]. The reorientation according to this model can be described by Eq. (A8) with the azimuth angle ϕ being time dependent. The condition $d(A_{\Omega=90°})/dt \approx d\langle\mu_x^2\rangle/dt=0$ is then just fulfilled, if all absorbance ellipsoids of the columns are uniaxial: $\langle\mu_\eta^2\rangle=\langle\mu_\zeta^2\rangle$. This uniaxiality is not in accordance with the biased rotational distribution of at least two of the transition moments assigned to the core (see above). Therefore, the second model is not appropriate to describe the observed reorientation behavior.

The rotation of the molecules around the column axis $\vec{N}$ [Fig. 11(c)] are described by Eq. (A6) with $\phi=\phi(t)$. Since $\langle\mu_x^2\rangle$ becomes time independent then, the observation $d(A_{\Omega=90°})/dt=0$ [Fig. 10(a)] can be explained within this third model. Similarly it can be shown that the application of Eq. (A6) leads to the observed modulations of the dichroic ratio and of the absorbance at an polarizer angle $\Omega = 45°$ [Fig. 10(b)].

Once it is known that the reorientation of the molecules takes place as a rotation around the column axis $\vec{N}$, one can use Eq. (A6) and the fitting data of the absorbances versus polarization plots A_Ω for all times t in order to determine the

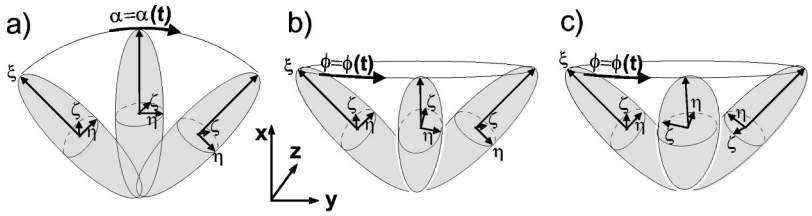

FIG. 11. Models for the reorientation path of a general absorbance ellipsoid. (a) Reorientation in the tilt plane. (b) Rotation of the disk normal only. (c) Rotation of the molecules on a cone around the column axis. Note the different behavior of the η and ζ axis in parts (b) and (c). The electric field is applied normal to the drawing plane. In this sketch ξ is the longest of the three axes. This does not coincide with the findings for the phenyl absorbance ellipsoids but is chosen for graphical reasons only.

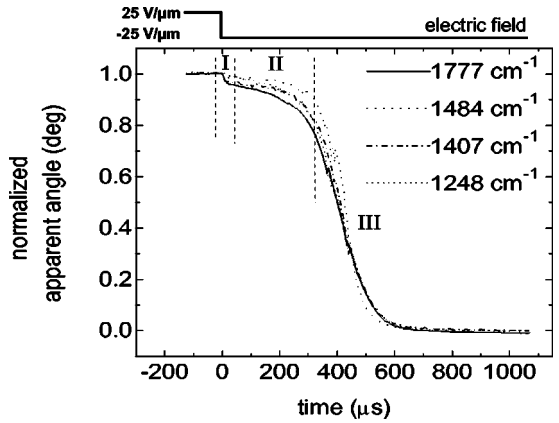

FIG. 12. Normalized time-resolved profiles for the apparent tilt angles for selected absorption bands of Fig. 7(a). The noncoincidence of these curves is not an equivocal proof of an asynchronous reorientation behavior of different molecular segments.

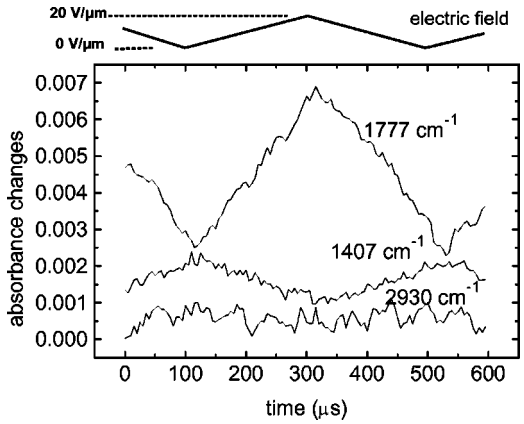

FIG. 13. Absorbance modulation for selected bands due to an electric field showing a linear response on application of a triangular voltage in the low-field phase. The time dependence of the external electric field is indicated.

biaxiality ($\langle\mu_\xi^2\rangle$, $\langle\mu_\eta^2\rangle$, and $\langle\mu_\zeta^2\rangle$) of the different absorbance ellipsoids (Table II). These results show different degrees of biaxiality for the bands assigned to the core. Two reasons for the biaxiality of the absorbance ellipsoids should be noted. First, the possibility of the disks to fluctuate along the tilt angle and along the tilt azimuth angle may be different, which usually is expressed by a transverse order parameter $D \neq 0$. Second, the transition moments in each single disk molecules may be asymmetrically distributed. Though the noncylindrical symmetry of the disk core is obvious (Fig. 2), an analysis of the distribution of the different transition moments in this core is beyond the aim of this paper.

The method for the determination of the reorientation path as done for the ferroelectric switching can also be applied to the fast initial reorientation process. From the facts that the $\langle\mu_x^2\rangle$ is not modulated and that the dichroic ratio decreases during this reorientation, one must conclude that this initial process is not electrocliniclike but can be described by a rotation of the discotic molecules around the column axis (i.e., on the tilt cone) by a few degrees. This process might be due to an inclination of the columnar axis with respect to the electrodes, similarly to the chevron structure observed in the Sm-C^* phase of calamitic liquid crystals. This result disproves our preliminary presumption of an electrocliniclike characteristic of this initial response that was reviewed in Ref. [17].

G. Synchronism of the molecular reorientation

In order to compare the time-resolved profiles of the apparent angles Ω_0 of different bands (Fig. 7), these values are normalized according to $\Omega_{0N}(t)=[\Omega_0(t)-\Omega_0(t>600\ \mu s)]/[\Omega_0(t<0)-\Omega_0(t>600\ \mu s)]$. The normalized curves as shown in Fig. 12 do not coincide with each other. Usually, a noncoincidence of the normalized time-dependent apparent angles of different bands is taken as a proof of asynchronous reorientation behavior of the corresponding molecular moieties [10,18,19]. Deviating from this interpretation, we found recently that such a noncoincidence can result from the geometry of the experiment alone [20]. Especially for tilted biaxial phases, a synchronous reorientation of molecular moieties can also lead to asynchronous responses of the time-resolved normalized apparent angles [20]. Hence, an unequivocal interpretation of the noncoincidence of the Ω_{0N} curves in Fig. 12 cannot be given here.

H. Orientation dynamics in the low-field phase

In the low-field phase the reorientation dynamics is also characterized by three different regions similar to that in the high-field phase: after a fast initial response in region I a plateau is formed in region II that is followed by a reorientation to a second surface stabilized state in region III. These results have been obtained by electro-optical measurements only. Unfortunately, due to technical limitations of our ir detector preamplifier we cannot follow the slow process in region III in the low-field phase by time-resolved FT-ir spectroscopy. For this reason only the initial fast response on the field reversal has been studied in this phase. The results shown in Fig. 13 are similar to that obtained for the high-field phase [Fig. 8(a)], the absorbance for selected bands changes linearly with voltage.

The mechanism of the reorientation in the low-field phase seems to be similar to that for the high-field phase: Both the fast and the ferroelectriclike reorientation take place by a rotation around the column axis $\vec{N}$. The fact that the initial response is faster than the subsequent reorientation shows that these two processes have different driving forces. Restoring elastic forces lead to an initial fast relaxation from an electrical induced structure with probably inclined column orientations. Compared to that the ferroelectriclike response is characterized by a comparatively slower reversal of the spontaneous polarization.

IV. CONCLUSION

FT-ir spectroscopy with polarized light enables one to elucidate the static arrangements in ferroelectric switchable discotic columnar liquid crystals. It was confirmed that in the low-field phase the columns differ by the orientation of their

disk normals with respect to the laboratory frame. In the high-field phase a homogeneous orientation of the columns is deduced. In both phases the alkyl tails are deflected with respect to the core planes.

Time-resolved FT-ir spectroscopy allows the possibility of following the reorientation dynamics under the influence of an alternating external electric field with a time resolution of 5 μs. It was detected that in both the high- and the low-field phases the reorientation from the first to the second state passes three regions: a fast initial response, a slowing down of the reorientation rate, and finally a second acceleration. Both the fast initial and the slower final reorientation to the second surface stabilized state are characterized by a rotation of the molecules around the columnar axis. A similar switching behavior is found in the low-field phase.

ACKNOWLEDGMENTS

The authors wish to thank H. Bock for the synthesis of the material Dm8*10. Financial support by Sfb 335 ''Anisotrope Fluide'' and the Innovationskolleg ''Phänomene an den Miniaturisierungsgrenzen'' is gratefully acknowledged. S.V.S. would like to thank the Alexander von Humboldt Foundation for an equipment donation.

APPENDIX

The dependence of the absorbance from the polarization vector $\vec{\epsilon}$ is expressed by an absorbance ellipsoid

$$A(\vec{\epsilon})=\langle(\vec{\mu}\vec{\epsilon})^2\rangle=\langle\mu_x^2\rangle\epsilon_x^2+\langle\mu_y^2\rangle\epsilon_y^2+\langle\mu_z^2\rangle\epsilon_z^2+2\langle\mu_x\mu_y\rangle\epsilon_x\epsilon_y+2\langle\mu_x\mu_z\rangle\epsilon_x\epsilon_z+2\langle\mu_y\mu_z\rangle\epsilon_y\epsilon_z \tag{A1}$$

where $\langle\mu_i\mu_j\rangle$ denotes the average value of the product of two components i and j of the infrared transition moments $\vec{\mu}$. By an appropriate coordinate transformation into the laboratory principle axis frame (L-PAF) Eq. (A1) simplifies to

$$A(\vec{\epsilon})=\langle(\vec{\mu}\vec{\epsilon})^2\rangle=\langle\mu_{x'}^2\rangle\epsilon_{x'}^2+\langle\mu_{y'}^2\rangle\epsilon_{y'}^2+\langle\mu_{z'}^2\rangle\epsilon_{z'}^2. \tag{A2}$$

If the phase contains n differently oriented columns it is useful to introduce also n absorbance ellipsoids for each type of column orientation. It should be noted that these n absorbance ellipsoids just differ in the orientation but not in the lengths of their axes. In other words, in each of their PAFs these n ellipsoids are identical. This columnar principle axis frame (C-PAF) should be denoted by ξ,η,ζ.

First we calculate how the orientation of the column and, therefore, the orientation of the C-PAF transforms into the laboratory coordinate system (laboratory frame LF). The LF can be defined by the plane in which the polarizer is rotated. This plane is parallel to the cell surface and is defined as the laboratory x-y plane. The polarizer angle $\Omega=90°$ defines the x axis, which is parallel to the axis of the columns. The y axis coincides with the ir polarization at $\Omega=0°$. The z axis is parallel to the ir beam propagation (Fig. 1). The simplest case deals with columns in which the core molecules are tilted in the x-y plane by an angle α with respect to the column axis [Fig. 11(a)]. Therefore, each transition moment that is described in the columnar principle axis frame of this type of column by the vector $(\mu_\xi,\mu_\eta,\mu_\zeta)^T$ is transformed into the laboratory frame $(x,y,z)^T$ by application of a rotation matrix

$$\begin{pmatrix}\mu_x\\ \mu_y\\ \mu_z\end{pmatrix}=D_\alpha^z\begin{pmatrix}\mu_\xi\\ \mu_\eta\\ \mu_\zeta\end{pmatrix}=\begin{pmatrix}c\alpha & -s\alpha & 0\\ s\alpha & c\alpha & 0\\ 0 & 0 & 1\end{pmatrix}\begin{pmatrix}\mu_\xi\\ \mu_\eta\\ \mu_\zeta\end{pmatrix}. \tag{A3}$$

The notation D_α^z represents a rotation around the axis z by an angle α and $s\alpha$ and $c\alpha$ are abbreviations for $\sin\alpha$ and $\cos\alpha$.

By averaging over all transition moments in this column type one obtains the parameters that describe the absorbance in the laboratory frame [Eq. (A1)],

$$\begin{aligned}\langle\mu_x^2\rangle&=\langle\mu_\xi^2\rangle\cos^2\alpha+\langle\mu_\eta^2\rangle\sin^2\alpha,\\ \langle\mu_y^2\rangle&=\langle\mu_\xi^2\rangle\sin^2\alpha+\langle\mu_\eta^2\rangle\cos^2\alpha,\\ \langle\mu_x\mu_y\rangle&=\{\langle\mu_\xi^2\rangle-\langle\mu_\eta^2\rangle\}\cos\alpha\sin\alpha,\end{aligned} \tag{A4}$$

and similar expressions for $\langle\mu_z^2\rangle$, $\langle\mu_x\mu_z\rangle$, and $\langle\mu_y\mu_z\rangle$. Here we made use of the fact that in the principle axis frame the equation $\langle\mu_\xi\mu_\eta\rangle=\langle\mu_\xi\mu_\zeta\rangle=\langle\mu_\eta\mu_\zeta\rangle=0$ is valid.

For a rotation of the absorbance ellipsoid around the column axis by an angle ϕ [Figs. 6(a), 11(c)], the transformation from the absorbance ellipsoid PAF into the laboratory system is performed by the successive application of two rotation matrices

$$\begin{pmatrix}\mu_x\\ \mu_y\\ \mu_z\end{pmatrix}=D_\phi^x D_\alpha^z\begin{pmatrix}\mu_\xi\\ \mu_\eta\\ \mu_\zeta\end{pmatrix}=\begin{pmatrix}c\alpha & -s\alpha & 0\\ c\phi s\alpha & c\phi c\alpha & -s\phi\\ s\phi s\alpha & s\phi c\alpha & c\phi\end{pmatrix}\times\begin{pmatrix}\mu_\xi\\ \mu_\eta\\ \mu_\zeta\end{pmatrix}, \tag{A5}$$

which leads to

$$\begin{aligned}\langle\mu_x^2\rangle&=\langle\mu_\xi^2\rangle\cos^2\alpha+\langle\mu_\eta^2\rangle\sin^2\alpha,\\ \langle\mu_y^2\rangle&=\langle\mu_\xi^2\rangle\sin^2\alpha\cos^2\phi+\langle\mu_\eta^2\rangle\cos^2\alpha\cos^2\phi+\langle\mu_\zeta^2\rangle\sin^2\phi,\\ \langle\mu_x\mu_y\rangle&=\{\langle\mu_\xi^2\rangle-\langle\mu_\eta^2\rangle\}\cos\alpha\sin\alpha\cos\phi.\end{aligned} \tag{A6}$$

Finally the cores axis but not the molecules themselves may be rotated by an angle ϕ around the x axis. That means that the molecules are no longer tilted initially in the x-y

plane and then are rotated along the x axis. Instead the molecules are tilted in a plane that forms an angle ϕ with respect to the x-y plane [Fig. 11(b)]. The corresponding transformation is described by

$$\begin{pmatrix} \mu_x \\ \mu_y \\ \mu_z \end{pmatrix} = D^x_{\phi} D^z_{\alpha} D^x_{-\phi} \begin{pmatrix} \mu_\xi \\ \mu_\eta \\ \mu_\zeta \end{pmatrix} \tag{A7}$$

$$= \begin{pmatrix} c\alpha & -s\alpha c\phi & -s\alpha s\phi \\ c\phi s\alpha & c^2\phi c\alpha + s^2\phi & c\phi s\phi(c\alpha - 1) \\ s\phi s\alpha & c\phi s\phi(c\alpha - 1) & s^2\phi c\alpha + c^2\phi \end{pmatrix} \begin{pmatrix} \mu_\xi \\ \mu_\eta \\ \mu_\zeta \end{pmatrix},$$

which leads to

$$\langle \mu_x^2 \rangle = \langle \mu_\xi^2 \rangle \cos^2\alpha + \langle \mu_\eta^2 \rangle \sin^2\alpha \cos^2\phi + \langle \mu_\zeta^2 \rangle \sin^2\alpha \sin^2\phi,$$

$$\langle \mu_y^2 \rangle = \langle \mu_\xi^2 \rangle \sin^2\alpha \cos^2\phi + \langle \mu_\eta^2 \rangle (\cos\alpha \cos^2\phi + \sin^2\phi)^2 + \langle \mu_\zeta^2 \rangle \sin^2\phi \cos^2\phi (\cos\alpha - 1)^2, \tag{A8}$$

$$\langle \mu_x \mu_y \rangle = \langle \mu_\xi^2 \rangle \cos\alpha \sin\alpha \cos\phi - \langle \mu_\eta^2 \rangle (\sin\alpha \cos\alpha \cos^3\phi + \sin\alpha \cos\phi \sin^2\phi) + \langle \mu_\zeta^2 \rangle (\sin\alpha - \sin\alpha \cos\alpha) \sin^2\phi \cos\phi.$$

For the low-field structures the absorbance ellipsoid in the LF is obtained by averaging the parameters $\langle \mu_x^2 \rangle$, $\langle \mu_y^2 \rangle$, and $\langle \mu_x \mu_y \rangle$ of Eq. (A6) over the different type of columns. For the structures of Type II [see Fig. 6(b)] one obtains: $\langle \mu_i \mu_j \rangle_{TypeII} = \frac{1}{6}\langle \mu_i \mu_j \rangle_{\phi=0^\circ} + \frac{1}{6}\langle \mu_i \mu_j \rangle_{\phi=180^\circ} + \frac{2}{6}\langle \mu_i \mu_j \rangle_{\phi=60^\circ} + \frac{2}{6}\langle \mu_i \mu_j \rangle_{\phi=300^\circ}$ with $i,j \in \{x,y,z\}$. Inserting the values according to Eq. (A6) results in

$$\langle \mu_x^2 \rangle_{TypeII} = \langle \mu_\xi^2 \rangle \cos^2\alpha + \langle \mu_\eta^2 \rangle \sin^2\alpha,$$

$$\langle \mu_y^2 \rangle_{TypeII} = \frac{1}{2}\langle \mu_\xi^2 \rangle \sin^2\alpha + \frac{1}{2}\langle \mu_\eta^2 \rangle \cos^2\alpha + \frac{1}{2}\langle \mu_\zeta^2 \rangle,$$

$$\langle \mu_x \mu_y \rangle_{TypeII} = \frac{1}{3}\{\langle \mu_\xi^2 \rangle - \langle \mu_\eta^2 \rangle\} \cos\alpha \sin\alpha, \tag{A9}$$

and similar expressions for $\langle \mu_z^2 \rangle$, $\langle \mu_x \mu_z \rangle$, and $\langle \mu_y \mu_z \rangle$. The same results are derived for the structures of Type I. The high-field phase contains only one type of columns, which is described by Eq. (A4).

During the reorientation in response to an external electric field the columns change their orientation. The three models that are discussed as possible reorientation mechanisms are described by Eq. (A4) under the assumption that the tilt angle α is changed during the reorientation and by Eq. (A6) and Eq. (A8) with $\phi = \phi(t)$, respectively.

For a comparison with the experimental results one has to take into account how the polarization vector $\vec{\epsilon}$ varies with the rotation angle Ω of the infrared polarizer. As the beam propagates along the laboratory z axis one gets

$$\vec{\epsilon} = \frac{\vec{E}}{|\vec{E}|} = \begin{pmatrix} \sin\Omega \\ \cos\Omega \\ 0 \end{pmatrix}, \tag{A10}$$

for which internal field effects are neglected.

Inserting Eq. (A10) into Eq. (A1) yields

$$A(\Omega) = \langle \mu_x^2 \rangle \sin^2\Omega + \langle \mu_y^2 \rangle \cos^2\Omega + 2\langle \mu_x \mu_y \rangle \cos\Omega \sin\Omega. \tag{A11}$$

By a coordinate transformation Eq. (A11) becomes

$$A(\Omega) = \langle \mu_{x'}^2 \rangle \cos^2(\Omega - \Omega_0) + \langle \mu_{y'}^2 \rangle \sin^2(\Omega - \Omega_0). \tag{A12}$$

Equations (A11) and (A12) are just valid for infinite thin samples. Taking a finite sample thickness into account Eq. (A12) must be rewritten [10,16]

$$A(\Omega) = -\log\{10^{-\langle \mu_{x'}^2 \rangle} \cos^2(\Omega - \Omega_0) + 10^{-\langle \mu_{y'}^2 \rangle} \sin^2(\Omega - \Omega_0)\} = -\log\{0.5(10^{-\langle \mu_{x'}^2 \rangle} + 10^{-\langle \mu_{y'}^2 \rangle}) + 0.5(10^{-\langle \mu_{x'}^2 \rangle} - 10^{-\langle \mu_{y'}^2 \rangle}) \cos 2(\Omega - \Omega_0)\}. \tag{A13}$$

Hence by fitting the polarizer dependent absorbance plots with

$$A(\Omega) = -\log\{f_1 + f_2 \cos 2(\Omega - \Omega_0)\}, \tag{A14}$$

one obtains the three parameters that describe the intersection of the absorbance ellipsoids with the plane normal to the beam propagation

$$\langle \mu_{x'}^2 \rangle = -\log\{f_1 + f_2\}, \langle \mu_{y'}^2 \rangle = -\log\{f_1 - f_2\} \quad \text{and} \quad \Omega_0. \tag{A15}$$

The coordinate transformation between the laboratory frame and the principle axis frame of the intersection (A11, A12) is performed according to

$$\langle \mu_x^2 \rangle = \langle \mu_{x'}^2 \rangle \sin^2\Omega_0 + \langle \mu_{y'}^2 \rangle \cos^2\Omega_0,$$

$$\langle \mu_y^2 \rangle = \langle \mu_{x'}^2 \rangle \cos^2\Omega_0 + \langle \mu_{y'}^2 \rangle \sin^2\Omega_0, \tag{A16}$$

$$\langle \mu_x \mu_y \rangle = (\langle \mu_{x'}^2 \rangle - \langle \mu_{y'}^2 \rangle) \cos\Omega_0 \sin\Omega_0,$$

and

$$\langle \mu_{x'}^2 \rangle = \frac{1}{2}(\langle \mu_x^2 \rangle + \langle \mu_y^2 \rangle) + \frac{1}{2}\sqrt{(\langle \mu_x^2 \rangle - \langle \mu_y^2 \rangle)^2 + (2\langle \mu_x \mu_y \rangle)^2},$$

$$\langle \mu_{y'}^2 \rangle = \frac{1}{2}(\langle \mu_x^2 \rangle + \langle \mu_y^2 \rangle) - \frac{1}{2}\sqrt{(\langle \mu_x^2 \rangle - \langle \mu_y^2 \rangle)^2 + (2\langle \mu_x \mu_y \rangle)^2},$$

$$\Omega_0 = \frac{1}{2}\arctan\frac{-2\langle \mu_x \mu_y \rangle}{\langle \mu_x^2 \rangle - \langle \mu_y^2 \rangle}, \tag{A17}$$

respectively.

[1] J. Prost, in *Comptes Rendus Du Colloque Pierre Curie: Symmetries and Broken Symmetries*, edited by N. Boccara (IDSET, Paris, 1981), p. 159.

[2] H. Bock and W. Helfrich, Liq. Cryst. **12**, 697 (1992).

[3] G. Scherowsky and X. H. Chen, Liq. Cryst. **17**, 803 (1994).

[4] G. Heppke, D. Krüerke, C. Löhning, D. Lötzsch, D. Moro, M. Müller, and H. Sawade, J. Mater. Chem. **10**, 2657 (2000).

[5] G. Heppke, D. Krüerke, M. Müller, and H. Bock, Ferroelectrics **179**, 203 (1996).

[6] H. Bock and W. Helfrich, Liq. Cryst. **18**, 387 (1995).

[7] G. Bogado, Ph.D. thesis, Freie Universität, Berlin, 1999.

[8] T. S. Perova, J. K. Vij, and H. Bock, Mol. Cryst. Liq. Cryst. **263**, 293 (1995).

[9] A. Kocot, G. Kruk, R. Wrzalik, and J. K. Vij, Liq. Cryst. **12**, 1005 (1992).

[10] F. Hide, N. A. Clark, K. Nito, A. Yasuda, and D. M. Walba, Phys. Rev. Lett. **75**, 2344 (1995).

[11] S. V. Shilov, H. Skupin, F. Kremer, T. Wittig, and R. Zentel, Phys. Rev. Lett. **79**, 1686 (1997).

[12] S. V. Shilov, E. Gebhard, H. Skupin, R. Zentel, and F. Kremer, Macromolecules **32**, 1570 (1999).

[13] H. Skupin, F. Kremer, S. V. Shilov, P. Stein, and H. Finkelmann, Macromolecules **32**, 3746 (1999).

[14] S. V. Shilov, H. Skupin, F. Kremer, K. Skarp, P. Stein, and H. Finkelmann, Proc. SPIE **3318**, 62 (1998).

[15] A. Jákli, M. Müller, D. Krüerke, and G. Heppke, Liq. Cryst. **24**, 467 (1998).

[16] A. Kocot, R. Wrzalik, B. Orgasinska, T. Perova, J. K. Vij, and H. T. Nguyen, Phys. Rev. E **59**, 551 (1999).

[17] T. S. Perova, J. K. Vij, and A. Kocot, in *Advances in Liquid Crystals*, special issue of Adv. Chem. Phys., edited by J. K. Vij (Wiley, New York, 2000), Vol. 113, p. 469–471.

[18] A. L. Verma, B. Zhao, S. M. Jiang, J. C. Sheng, and Y. Ozaki, Phys. Rev. E **56**, 3053 (1997).

[19] A. L. Verma, B. Zhao, H. Terauchi, and Y. Ozaki, Phys. Rev. E **59**, 1868 (1999).

[20] H. Skupin, Ph.D. thesis, University of Leipzig, 2001.